RSC Advances

PAPER

View Article Online
View Journal | View Issue

Cite this: *RSC Adv.*, 2021, **11**, 18797

Ultrafast conversion of carcinogenic 4-nitrophenol into 4-aminophenol in the dark catalyzed by surface interaction on $BiPO_4/g\text{-}C_3N_4$ nanostructures in the presence of $NaBH_4$†

Ahmed B. Azzam, *[a] Ridha Djellabi,[b] Sheta M. Sheta [c] and S. M. El-Sheikh [d]

The heterogeneous catalytic conversion of pollutants into useful industrial compounds is a two-goals at once process, which is highly recommended from the environmental, economic, and industrial points of view. In this regard, design materials with high conversion ability for a specific application is required to achieve such a goal. Herein, the synthesis conditions for the fabrication of $BiPO_4$ nanorod bundles supported on $g\text{-}C_3N_4$ nanosheets as heterojunction composites was achieved using a facile *ex situ* chemical deposition for the reductive conversion of carcinogenic 4-nitrophenol (4-NP) into 4-aminophenol (4-AP). To better understand the mechanistic reduction pathways, $BiPO_4/g\text{-}C_3N_4$ composites with varying ratios where obtained. The morphology and structure of $BiPO_4/g\text{-}C_3N_4$ composites were checked using several methods: XRD, FE-SEM, HRTEM, XPS, and FT-IR, and it was found that hexagonal phase $BiPO_4$ nanorod bundles were randomly distributed on the $g\text{-}C_3N_4$ nanosheets. Overall, the reduction ability of $BiPO_4/g\text{-}C_3N_4$ composites was far better than bare $BiPO_4$ and $g\text{-}C_3N_4$. A total reductive conversion of 4-NP at a concentration of 10 mg L^{-1} into 4-AP was found with 50% $BiPO_4/g\text{-}C_3N_4$ composite within only one minute of reaction. Moreover, the presence of reducing agent ($NaBH_4$) enhanced the kinetic rate constant up to 2.914 min^{-1} using 50% $BiPO_4/g\text{-}C_3N_4$, which was much faster than bare $BiPO_4$ (0.052 min^{-1}) or $g\text{-}C_3N_4$ (0.004 min^{-1}). The effects of some operating parameters including the initial concentration of 4-NP and catalyst dosage were also evaluated during the experiments. $BiPO_4/g\text{-}C_3N_4$ showed great stability and recyclability, wherein, the catalytic reduction efficiency remains the same after five runs. A plausible 4-NP reduction mechanism was discussed. The high catalytic activity with the good stability of $BiPO_4/g\text{-}C_3N_4$ make it a potential candidate for the reduction of nitroaromatic compounds in real wastewaters.

Received 12th April 2021
Accepted 18th May 2021

DOI: 10.1039/d1ra02852a

rsc.li/rsc-advances

1. Introduction

Petrochemical and pesticide manufacturing industries discharge huge amounts of nitroaromatic compounds, *e.g.*, nitrophenols, which are known as potential environmental hazards to human health because of their high degree of carcinogenic risk and non-biodegradability in the aquatic or/and soil environments.[1,2] Many efforts have been made to remove nitrophenols from the environment using different physicochemical or photonic techniques.[3–7] Of these, the reduction of nitrophenol is a great strategy as it achieves two goals at the same time, including the removal of toxic compound from the medium, plus the production of aminophenol as a valuable compound for industrial use such as in pharmaceutical and drug processing.[8] Therefore, the intensification of green technologies for enhanced and selective reduction of nitrophenol into aminophenol has received much attention recently due to the important environmental and economic impact.[9,10] In this regard, over the last decades, semiconductor catalysts have attracted wide attention for removing environmental pollutants or/and converting them into useful compounds for industrial use.[11,12] Numerous semiconductor materials with appropriate physicochemical or/and photochemical properties have been widely developed and used for the catalytic and photocatalytic transformation of compounds.[13,14]

[a]*Faculty of Science, Chemistry Department, Helwan University, Ain Helwan, Cairo 11795, Egypt. E-mail: ahmed_azzam2000@hotmail.com; Tel: +201285259709*
[b]*Università degli Studi di Milano, Dip. Chimica and INSTM-UdR Milano, Via Golgi, 19, 20133 Milano, Italy*
[c]*Department of Inorganic Chemistry, National Research Centre, 33, El-Behouth St., Dokki, Giza 12622, Egypt*
[d]*Nanomaterials and Nanotechnology Department, Advanced Materials Division, Central Metallurgical R & D Institute (CMRDI), P. O. Box, 87 Helwan, 11421 Cairo, Egypt*

† Electronic supplementary information (ESI) available. See DOI: 10.1039/d1ra02852a

g-C_3N_4 has been considered as one of the most successful π-conjugated polymers over the last decades, due to its high stability, good absorption in the visible light and photo-efficiency.[15] Owing to the existence of the lamellar structure, g-C_3N_4 is always well-crystallized, allowing the transfer of charges.[16] In view of its unique structure, and photochemical characteristics, g-C_3N_4 has been widely employed in various fields, for instance, removal of pollutants from water or air,[17] reduction of hazardous metals,[18] water splitting,[19] hydrogen evolution.[20] Therefore, g-C_3N_4 as a metal-free material is identified to be a "sustainable develop" catalyst. Regardless, the photocatalytic effectiveness of g-C_3N_4 is still limited due to several issues including the fast recombination of electron/hole charges and low adsorption capacity.[21,22] To limit the recombination of charges and enhance the catalytic ability of g-C_3N_4, the surface modification though metal doping[23] or non-metal doping processes[24] were extensively reported. In terms of 4-nitrophenol reduction, Pd, Ag, Au doped g-C_3N_4 have been utilized to improve the catalytic activity of 4-nitrophenol reduction.[25–28] On top of that, the combination of g-C_3N_4 with other semiconductors to form heterojunction systems which gives a range of synergistic benefits, wherein, the interfacial charge-transfer (IFCT) is the key advantage as it can enhance significantly the yield of long lifetime of separated redox charge carriers.[29,30] For a successful construction of a heterojunction systems, the semiconductors should be properly chosen. In recent decades, the scientific community has addressed widely the application of bismuth based nanomaterials such as BiOBr, Bi_2S_3, $BiPO_4$, $BiVO_4$, Bi_2WO_6, $Bi_2O_2CO_3$ in different catalytic applications thanks to their appropriate physicochemical and photonic characteristics.[31–36] In particular, $BiPO_4$ as a new bismuth salt catalyst, which has been developed for the first type by Zhu's group, has been revealed as promising candidate in semiconductor catalysis due to its highly photocatalytic efficiency under UV light which was found to be superior that TiO_2 (P25, Degussa) towards the oxidation of dyes.[37] However, the catalytic performance of $BiPO_4$ has been greatly restricted. Like other semiconductors, a lot research has been carried out on $BiPO_4$ to improve its (photo)-catalytic efficiency and visible light response. One of the used strategies is the combination of $BiPO_4$ with other semiconductors to get multifunctional heterojunctions with combined options, which could enhance the surface interactions, charges transfer and better visible light response.[38–40] Other ways have been also reported including surface hybridization with π-conjugated materials,[41–43] creation of surface oxygen vacancies,[44,45] and phase junction system.[46,47] The combination of g-C_3N_4 with $BiPO_4$ has been proved to be very successful due to the excellent interfacial interaction between the two nanostructured materials in terms of high yield of separated charged and enhanced (photo)-catalytic reactions.[48–50] However, the catalytic reduction application and mechanism of heterojunction $BiPO_4$ with g-C_3N_4 have not been thoroughly investigated.

In this work, we report the fabrication of $BiPO_4$ nanorod bundles/g-C_3N_4 nanosheets composite architectures with ultrafast catalytic efficacy towards the reduction of 4-nitrophenol. As far as we know, this is the first investigation on the use of $BiPO_4$/g-C_3N_4 to initiate the reduction of 4-NP in dark condition. The catalytic efficiencies bare $BiPO_4$ and g-C_3N_4 were studied as well for the purpose of comparison. Additionally, the effect of different $BiPO_4$:g-C_3N_4 ratios on the catalytic effectiveness was checked. The effect of some operating parameters such as the initial concentration of 4-NP and catalyst amount on the catalytic performance was studied. The stability of $BiPO_4$/g-C_3N_4 composite and the feasible mechanistic pathway for the catalytic reduction of 4-NP were addressed.

2. Experimental

All chemicals and characterization instruments were reported in the ESI.†

2.1 Synthesis of $BiPO_4$ nanorod bundles

The details of the synthesis of $BiPO_4$ were reported in our previous study.[51] Typically, 1.94 g of $Bi(NO_3)_3 \cdot 5H_2O$ and 0.5 g CTAB were stirred in 40 mL dimethyl sulfoxide. Then 0.524 g $(NH_4)_2HPO_4$ dissolved in 40 mL of water was dropped into the previous solution under vigorous stirring for 1 h. After the formation of precipitate, the solid was recovered with centrifugation, and then washed with water and ethanol, and finally it was dried for 6 h at 90 °C.

2.2 Synthesis of g-C_3N_4 nanosheets

g-C_3N_4 was synthesized through the direct hearting of mixture of melamine and urea (5 : 5 g) at 600 °C in a muffle furnace for 2 h with 2 °C min^{-1} heating rate. The obtained yellow solid was ground.

2.3 Synthesis of $BiPO_4$ nanorod bundles/g-C_3N_4 nanosheets

To develop $BiPO_4$/g-C_3N_4 heterojunction photocatalyst, the *ex situ* route was adopted, as shown in Scheme 1, the growth of

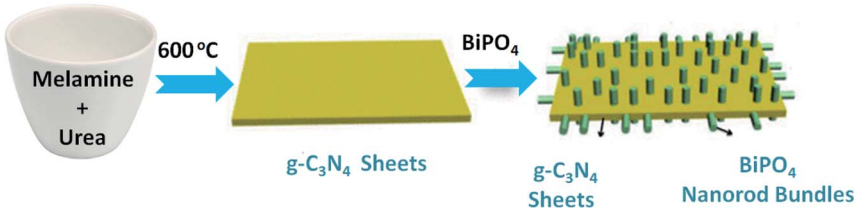

Scheme 1 Diagram representation for the synthesis and structure of $BiPO_4$/g-C_3N_4 heterojunction.

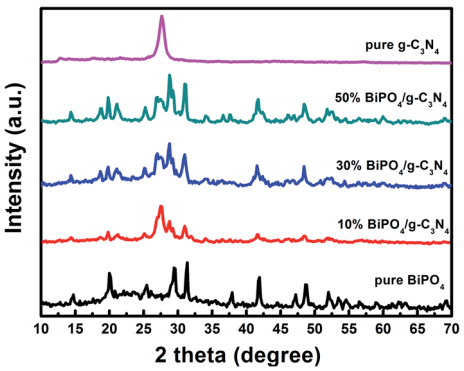

Fig. 1 Powder XRD patterns of pure $BiPO_4$, g-C_3N_4, 10% $BiPO_4$/g-C_3N_4, 30% $BiPO_4$/g-C_3N_4, and 50% $BiPO_4$/g-C_3N_4.

$BiPO_4$ nanorod bundles within sheets of g-C_3N_4 was obtained. In details, 0.5 g of g-C_3N_4 was mixed with 50 mL methanol and stirred for 1 h. Different amounts of $BiPO_4$ was ultrasonically dispersed into g-C_3N_4 suspension for 10 min and complete stirring for 1 h to denote as 10% $BiPO_4$/g-C_3N_4, 30% $BiPO_4$/g-C_3N_4, 50% $BiPO_4$/g-C_3N_4, and 70% $BiPO_4$/g-C_3N_4 samples. Finally, the composites were washed with water and dried for 6 h at 90 °C.

2.4 Catalytic reduction test of 4NP

The catalytic behavior was investigated towards the reductive conversion of 4-nitrophenol into 4-aminophenol in the presence of $NaBH_4$. First, 50 mL of an aqueous solution of 4-nitrophenol (10 ppm) was mixed with $NaBH_4$ (16 mM), which leads to form a strong yellow solution. Then, 25 mg of the catalyst was added in dark to yellow solution and the reaction was performed until the solution became colorless. A 3 mL aliquots were taken at different time intervals, and the solid suspension was removed *via* centrifugation. The concentration of compounds was followed by the use of UV-vis spectrophotometer. The recycling of $BiPO_4$/g-C_3N_4 was carried out to check the stability. For this, the catalyst was recovered after the reaction, and the washed with double distilled water and dried at 90 °C for subsequent tests.

3. Results and discussion

3.1 Characterization

Fig. 1 illustrates the XRD patterns of bare $BiPO_4$, g-C_3N_4, and $BiPO_4$/g-C_3N_4 hybrid composites. The diffraction peaks of $BiPO_4$ at 2-theta angles 14.7°, 20.1°, 25.5°, 29.5°, 31.3°, 41.9°, and 48.7° which corresponding to the crystal orientations of (100), (101), (110), (200), (102), (211), and (212) planes of $BiPO_4$. These diffraction peaks correspond to JCPDS card no. 15-0766.[52] It can be seen from the diffraction peaks that $BiPO_4$ is a hexagonal phase (HBIP, space group: $P3_121$). g-C_3N_4 pattern shows an intense peak at $2\theta = 27.7°$ corresponding to its crystal plane (002) of stacking conjugated aromatic system, while the peak at 12.9° is due to the tristriazine units.[53] The diffraction peaks of g-C_3N_4 from mixture of urea and melamine is more intense than as prepared by urea as shown in Fig. S1.† No other peaks or impurities are observed, implying that the final products of $BiPO_4$ and g-C_3N_4 are of pure phases. The diffraction pattern of $BiPO_4$/g-C_3N_4 shows that the composite is composed of the hexagonal phase $BiPO_4$ and g-C_3N_4. The intensity of diffraction peaks of $BiPO_4$ are gradually strengthen with increasing $BiPO_4$ content. Consequently, the above results confirm the successful formation $BiPO_4$/g-C_3N_4 heterojunction.

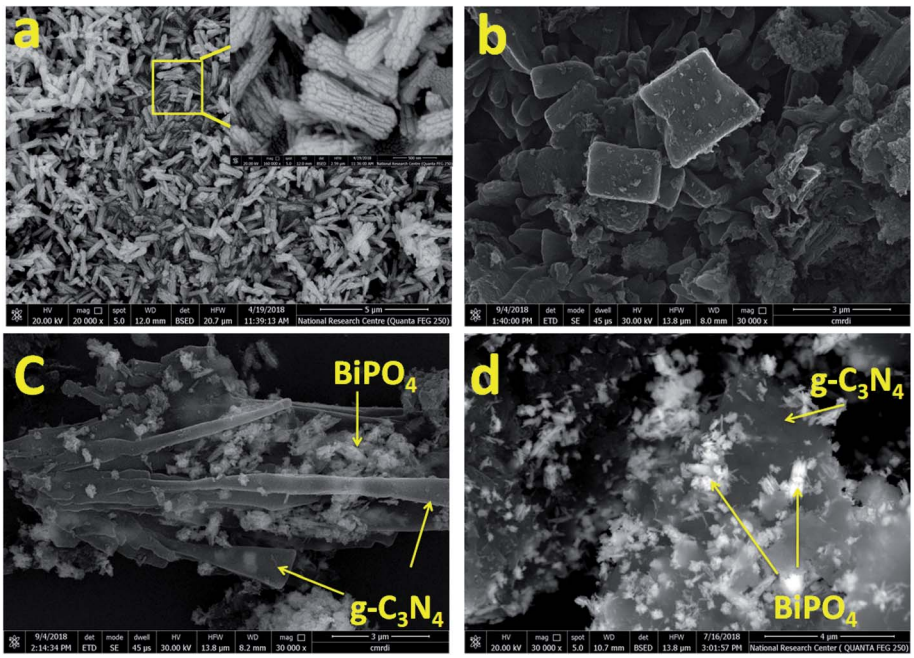

Fig. 2 FE-SEM images of $BiPO_4$ (a), g-C_3N_4 (b), and 30% $BiPO_4$/g-C_3N_4 (c), and 50% $BiPO_4$/g-C_3N_4 (d).

The surface morphologies of bare $BiPO_4$, g-C_3N_4, 30% $BiPO_4$/g-C_3N_4, and 50% $BiPO_4$/g-C_3N_4 catalysts were characterized by FE-SEM. As depicted in Fig. 2, the diameter of nanorod bundles in $BiPO_4$ was found to be 300 nm, and lengths of 800 nm (Fig. 2a). Whereas the g-C_3N_4 displayed a typical sheet-like morphology with several crystallites (Fig. 2b). After the heterojunction was successfully formed in 30% $BiPO_4$/g-C_3N_4, and 50% $BiPO_4$/g-C_3N_4 samples, the agglomeration of $BiPO_4$ could be observed by the insertion of $BiPO_4$ nanorods bundles in the inter sheets of g-C_3N_4 (Fig. 2c and d), which implies that the g-C_3N_4 sheets are coated with $BiPO_4$ nanorods bundles.

The TEM image (Fig. 3a) revealed that $BiPO_4$ was composed of nanorods with diameter ranging from 30 to 40 nm. HRTEM (Fig. 3b) showed that $BiPO_4$ nanorod bundles have a lattice fringe spacing of 0.349 nm, which can be indexed to (110) crystal plane of $BiPO_4$ (JCPDS card no. 15-0766). The SAED pattern (Fig. 3c) confirmed the polycrystalline nature of the material due to the presence of concentric ring shape like. The TEM images shown in Fig. 3d indicated that $BiPO_4$ nanorod bundles are bonded to g-C_3N_4 nanosheets. HRTEM (Fig. 3e) shows a fringe spacing of 0.350 nm due to (110) crystal planes of $BiPO_4$. In addition, the polycrystalline phase was observed in SAED pattern (Fig. 3f). It can be seen from TEM images (Fig. 3g) that g-C_3N_4 has an unsmooth surface, which could boost the catalytic reaction by offering a higher surface area or/and favorizes the immobilization of other semiconductor nanoparticles. From the results of materials characterization, it can be concluded that the $BiPO_4$ nanorod bundles was successfully immobilized on the g-C_3N_4 nanosheets to form heterojunction system.

The chemical oxidation state of $BiPO_4$/g-C_3N_4 hybrid structure was verified using XPS analysis. Fig. 4a illustrates the full scan survey which indicate the presence of Bi, P, O, C and N elements, implying the successful heterojunction of $BiPO_4$ and g-C_3N_4. The high resolution Bi 4f, P 2p, O 1s, C 1s, and N 1s are shown in Fig. 4b–f. The binding energies peaks at 159.81 eV and 165.11 eV (Fig. 4b) are due to the Bi $4f_{7/2}$ and Bi $4f_{5/2}$ levels in $BiPO_4$, respectively.[54] The Bi $4f_{7/2}$ and Bi $4f_{5/2}$ peaks showed

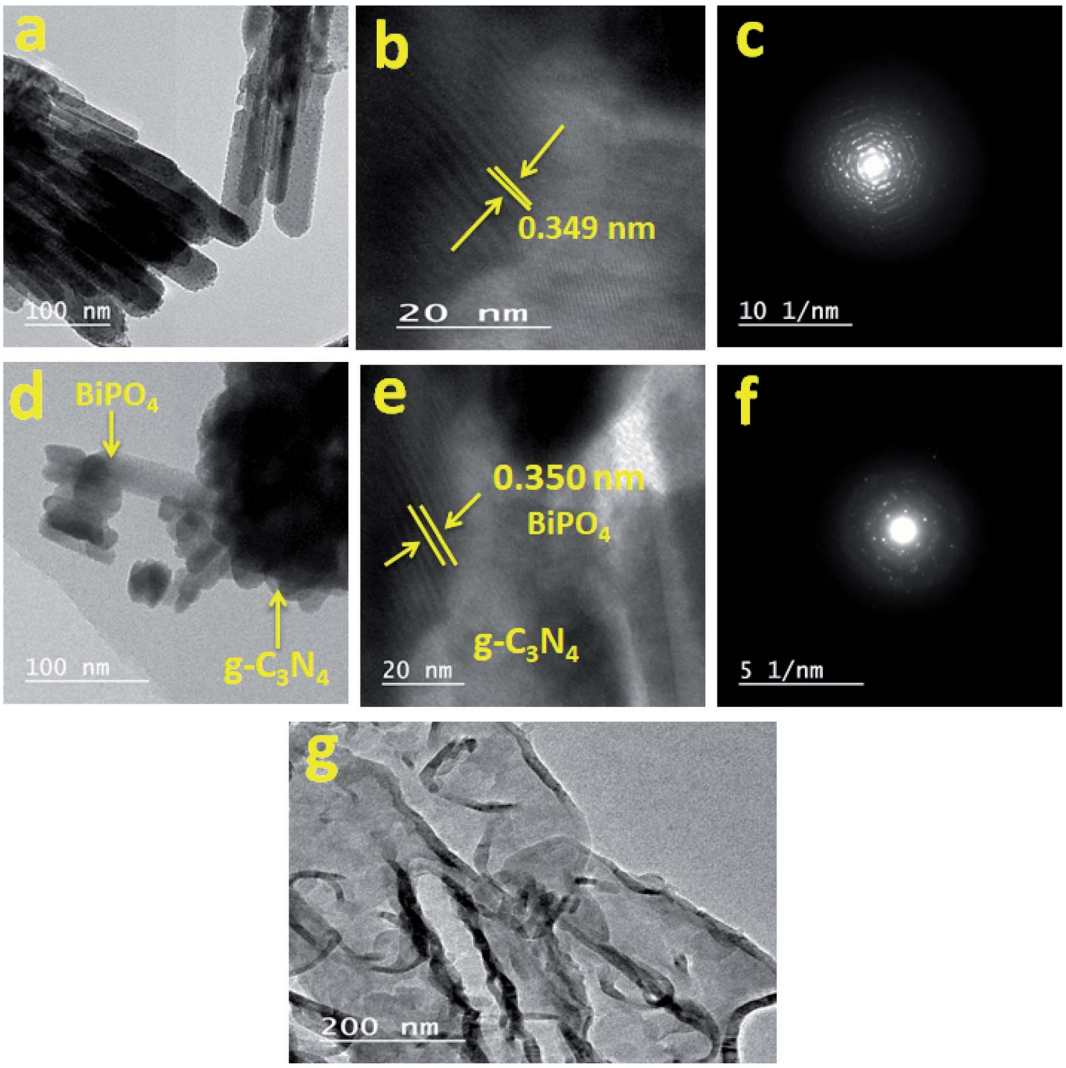

Fig. 3 TEM, HRTEM images and SEAD pattern of $BiPO_4$ (a, b, and c, respectively), $BiPO_4$/g-C_3N_4 hybrid structure (d, e, and f, respectively), and TEM image of g-C_3N_4 (g).

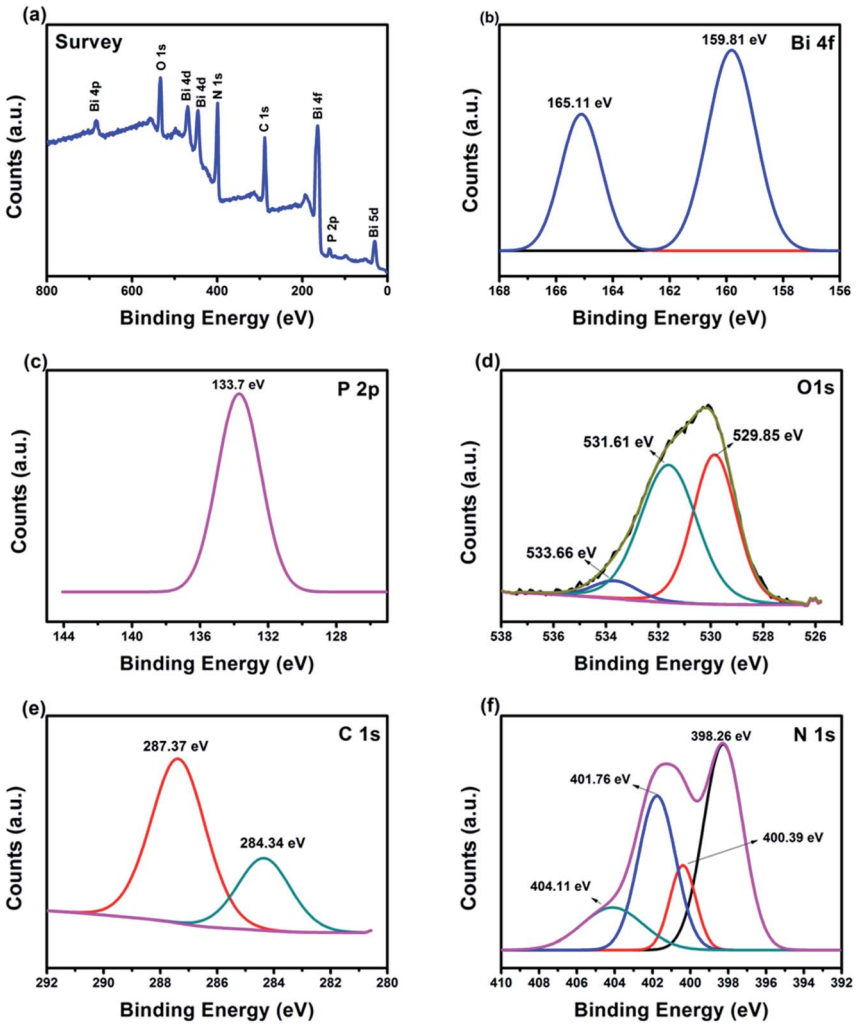

Fig. 4 XPS spectra of $BiPO_4$/g-C_3N_4, (a) survey spectra, (b) Bi 4f, (c) P 2p, (d) O 1s, (e) C 1s, (f) N 1s.

a splitting of 5.3 eV which confirms that Bi atoms have a valence state of +3.[55] The characteristic peak of P 2p can be found at 133.7 eV (Fig. 4c), which ascribed to the P^{5+} in $BiPO_4$.[56] In Fig. 4d, the peaks at 529.85, 531.61 and 533.66 eV correspond to O^{2-} bonded to Bi, surface bound and adsorbed oxygen, respectively.[57] The two peaks in C 1s spectra appeared at 284.34 and 287.37 eV are due to the sp^2 bonded carbon atoms such as carbon–carbon bonding (C–C), and carbon–nitrogen double bond (C=N), respectively (Fig. 4e).[58,59] The high resolution N 1s XPS spectra in Fig. 4f is divided into four bands with energies of 398.26, 400.39, 401.76 and 404.11 eV correspond to C–N=C, N–$(C)_3$ groups, and $(C)_2$–N–H, respectively.[50,60] The XPS data is an accordance with XRD, FE-SEM, and TEM analysis.

FTIR spectra of bare semiconductors and $BiPO_4$/g-C_3N_4 composites are shown in Fig. 5. In terms of $BiPO_4$, bending vibration peaks due to PO_4 group are detected at 587 and 534 cm^{-1}. The band at 974 cm^{-1} is assigned to PO_4 stretching vibration.[41] The band at 3495 cm^{-1} corresponds to hydroxyl stretching vibration groups of the surface adsorbed or/and structure water molecules in $BiPO_4$. δ(H–O–H) bending vibrations can be observed also at 1602 cm^{-1}. g-C_3N_4 spectrum shows a large band at 3155 cm^{-1} as a result of stretching vibration in NH and NH_2 groups.[61] The heptazine heterocyclic ring stretching vibrations in g-C_3N_4 units were appeared at 1200–1650 cm^{-1}. In addition, the peaks at 1310 and 1629 cm^{-1} correspond respectively to the stretching vibrations of C–N and C=N.[61] The characteristic peak at about 800 cm^{-1} could be assigned to the triazine units.[62] For $BiPO_4$/g-C_3N_4 samples, the

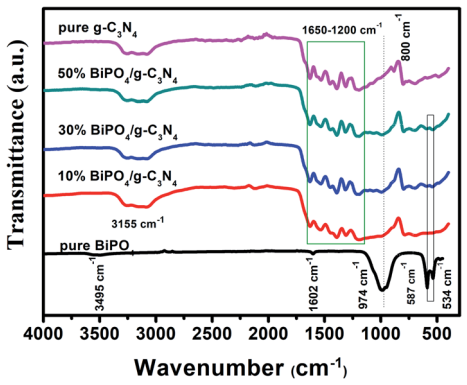

Fig. 5 FT-IR spectra of pure $BiPO_4$, g-C_3N_4, 10% $BiPO_4$/g-C_3N_4, 30% $BiPO_4$/g-C_3N_4, and 50% $BiPO_4$/g-C_3N_4.

entire characteristic peaks of (PO_4) group (bending, stretching vibration) in $BiPO_4$ are gradually strengthen with increasing $BiPO_4$ content, implying that the $BiPO_4$ and g-C_3N_4 are of harmonious coexistence.

3.2 4-NP catalytic reduction

The catalytic performances of as-prepared catalysts towards the reduction of 4-NP to 4-AP in the presence of $NaBH_4$ are shown in Fig. 6. The maximum absorption peak of aqueous solution of 4-NP (Fig. 6a) is shown at 318 nm but after addition of $NaBH_4$ the peak shifted to 400 nm with a color conversion from light yellow to strong yellow due to $NaBH_4$ converted 4-nitrophenol to 4-nitrophenolate.[63,64] The coexistence of these two peaks indicates the copresence of 4-nitrophenol and nitrophenolate during the equilibrium, which is due to 4-nitrophenol self-ionization.[10] In terms of g-C_3N_4, no significant reduction was observed for pure g-C_3N_4 in presence of $NaBH_4$ (Fig. 6b). As seen in Fig. 6c–f, when 0.5 g L^{-1} of $BiPO_4$/g-C_3N_4 composite was added to the reaction medium, a fast disappearance of yellow color was found, and

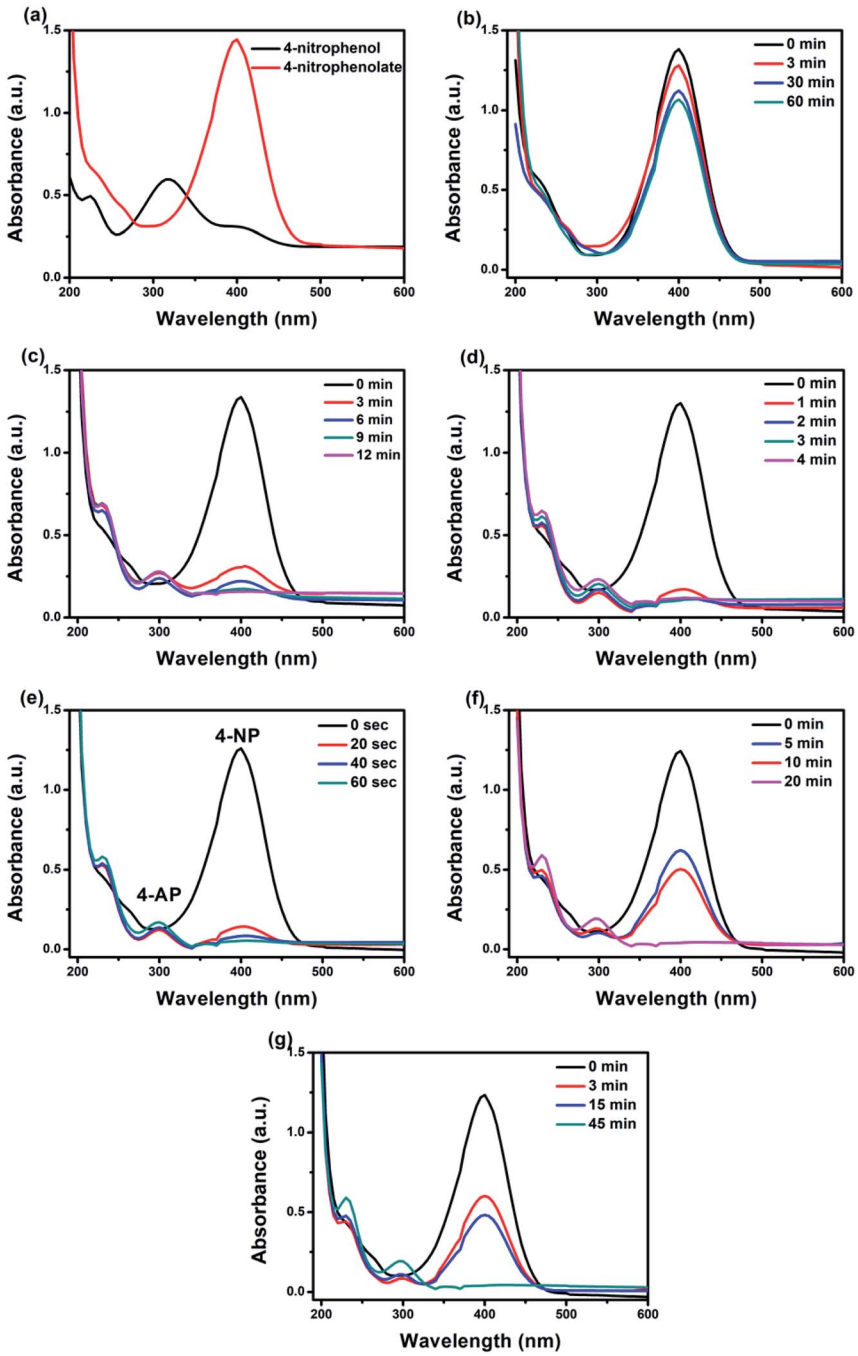

Fig. 6 UV-vis spectral changes of 4-NP before and after adding $NaBH_4$ solution (a); the successive reduction of 4-NP to 4-AP in presence of pure g-C_3N_4 (b), 10% $BiPO_4$/g-C_3N_4 (c), 30% $BiPO_4$/g-C_3N_4 (d), 50% $BiPO_4$/g-C_3N_4 (e), 70% $BiPO_4$/g-C_3N_4 (f) and pure $BiPO_4$ (g). ([4-NP] = 10 mg L^{-1}, [catalyst] = 0.5 g L^{-1}).

a quick decrease in the peak intensity of 400 nm, and at the same time the characteristic peak of 4-AP at 300 nm was appeared, reflecting the reduction reaction.[65] Time consumed for reduction of 4-NP is 12, 4, 1, and 20 min for 10% $BiPO_4$/g-C_3N_4, 30% $BiPO_4$/g-C_3N_4, 50% $BiPO_4$/g-C_3N_4, and 70% $BiPO_4$/g-C_3N_4, respectively. In addition, bare $BiPO_4$ showed similar spectral tendency within 45 min (Fig. 6g). The order of the catalytic performances was as follows 50% $BiPO_4$/g-C_3N_4 > 30% $BiPO_4$/g-C_3N_4 > 10% $BiPO_4$/g-C_3N_4 > 70% $BiPO_4$/g-C_3N_4 > $BiPO_4$ > g-C_3N_4. Increasing percentage of $BiPO_4$ to 70% may cover surface of g-C_3N_4 and decreased the catalytic reduction of 4-NP. The enhancement of catalytic performance ability could be attributed to the synergistic heterojunction effect between $BiPO_4$ and g-C_3N_4 nanosheets, high electrical conductivity, and enlarged reaction active sites.

The reduction conversion kinetics of 4-NP were studied by the first-order simplification of Langmuir–Hinshelwood (L–H), using the following equation:[66]

$$\ln(A_t/A_0) = -k_{app}t$$

Table 1 The k_{app} values for the reduction of 4-nitrophenol with and without catalysts in the presence of $NaBH_4$

S. No.	Catalyst	K_{app} (min^{-1})
1	C_3N_4	0.004
2	10% $BiPO_4$/g-C_3N_4	0.186
3	30% $BiPO_4$/g-C_3N_4	0.677
4	50% $BiPO_4$/g-C_3N_4	2.914
5	70% $BiPO_4$/g-C_3N_4	0.13
6	$BiPO_4$	0.052
7	Without catalyst	0.001

where A_0 and A_t are absorbance of 4-NP in solution at times 0 and t, respectively, and k is the first-order rate constant (min^{-1}). The k_{app} value is obtained from a liner plot of $\ln(A_t/A_0)$ *versus* time (t), as shown in Fig. 7e. The rate constant values was 0.004, 0.052, 0.186, 0.677, and 2.914 min^{-1} for pure g-C_3N_4, $BiPO_4$, 10% $BiPO_4$/g-C_3N_4, 30% $BiPO_4$/g-C_3N_4, 50% $BiPO_4$/g-C_3N_4, and 70% $BiPO_4$/g-C_3N_4, respectively as shown in Fig. 7e

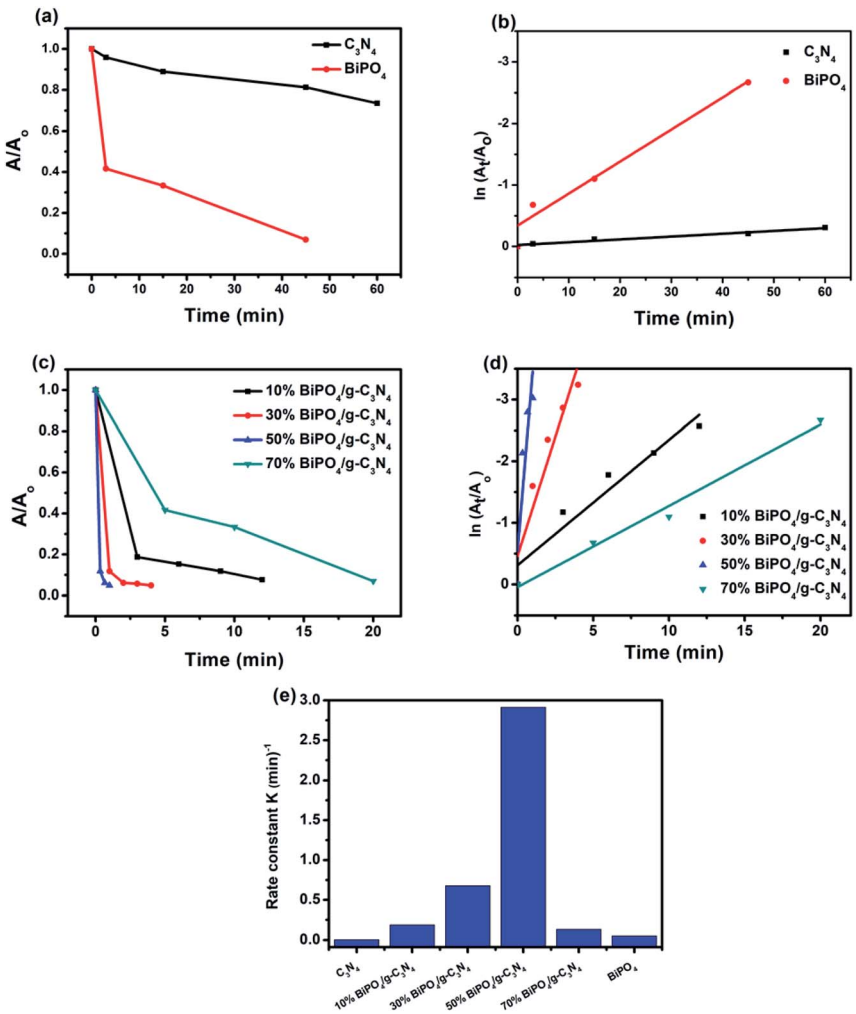

Fig. 7 Reduction rate of 4-NP over different catalysts (a and c); corresponding linear transform $\ln(A/A_0) = f(t)$ of the 4-NP reduction kinetics curves (b and d); comparison of the rate constant value for the reduction of the 4-NP over different catalysts (e). ([4-NP] = 10 mg L^{-1}, [catalyst] = 0.5 g L^{-1}).

Table 2 Impact of temperature on k_{app} values for the reduction of 4-nitrophenol ([4-NP] = 30 mg L^{-1}, [catalyst] = 0.5 g L^{-1})

S. No.	Temperature (K)	K_{app} (min^{-1})
1	298	1.1
2	303	1.25
3	308	3.50
4	313	4.67
5	318	5.24

and Table 1. It is clear the increase of the amount of $BiPO_4$ in the composite leads to increase proportionally the rate constant of the reduction reaction. Therefore, 50% $BiPO_4$/g-C_3N_4 sample gives the highest k value which was 728.5 and 56 times superior than the values recorded for g-C_3N_4 and $BiPO_4$, respectively. The impact of temperature on reduction of 4-NP was further investigated using 50% $BiPO_4$/g-C_3N_4. The k_{app} values improved with the increase in temperature due to increasing diffusion rate of reactant molecules (Table 2).

The turnover number (TON) and the turn over frequency (TOF) of 50% $BiPO_4$/g-C_3N_4 heterojunction have been further investigated to show the catalytic efficiency of the catalyst. The TON of catalyst is the number of 4-NP molecules that can convert into products using 1 g of catalyst, while TOF is calculated as TON/time. The concentration of 4-NP and dosage of catalyst are 7.18×10^{-5} M, 0.025 g, respectively. The TOF was found to be 0.249 molecules per g.s for 50% $BiPO_4$/g-C_3N_4 heterojunction using the following equation:[64]

$$\mathrm{TOF} = \frac{m_i X x}{100\ Wt}$$

where m_i is the initial number of moles nitrophenol, X is the conversion of 4-NP, x is the molecular weight of 4-NP, W is the mass of catalyst used in the reaction (g), and t is the reaction time (h).

3.2.1 Effect of initial concentration of 4-NP. The effect of initial concentration of 4-NP on the catalytic efficiency rate using 50% $BiPO_4$/g-C_3N_4 catalyst was carried by varying the concentration from 10 to 70 mg L^{-1}, and the obtained results as shown in Fig. 8a. Interestingly, 50% $BiPO_4$/g-C_3N_4 was able to reduce all 4-NP solutions at concentrations from 10 to 70 mg L^{-1} reflecting the highly efficiency of such a catalyst towards this 4-NP reduction. At lower concentration, superior constant rate was recorded due to the availability of large number of catalytic sites per a given amount of 4-NP moles. And *vice versa*, the higher the concentration, the lower the rate constant (Fig. 8b) fitting pseudo-first-order reaction, due to the high competition of 4-NP molecules on the limited sites. In addition, the number of molecules adsorbed at the surface of the $BiPO_4$/g-C_3N_4 heterojunction increases with the increase in the concentration of 4-nitrophenol and hence, the surface becomes saturated by 4-nitrophenol molecules. This leads to a decrease in concentration of BH_4^- ions approaching the surface of the $BiPO_4$/g-C_3N_4 heterojunction, hence lowering the rate of hydrogen transfer from BH_4^- ion to the 4-nitrophenol molecule. This confirms that the $BiPO_4$/g-C_3N_4 catalyzed reduction of nitrophenol occurs according to the L–H mechanism.

3.2.2 Effect of catalyst amount. We also investigated the effect of catalyst dosage (0.012–0.05 g) on the reduction 4-NP (70 mgL^{-1}). As seen in Fig. 9, with the increase of catalyst dosage, the removal efficiency of 4-NP improved markedly. With further

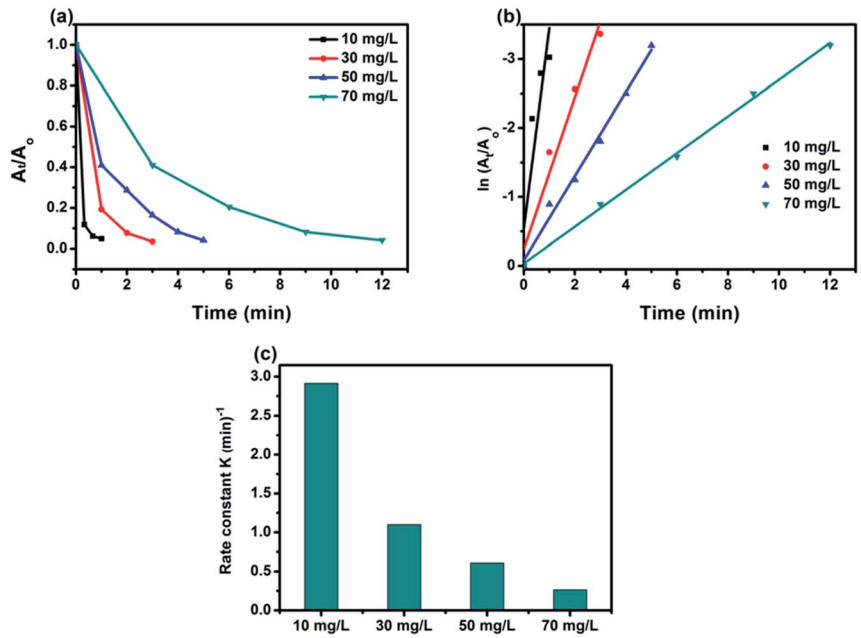

Fig. 8 Effect of initial concentration on reduction rate of 4-NP (a); corresponding linear transform $\ln(A_t/A_0) = f(t)$ of the 4-NP reduction kinetics curves (b); comparison of the rate constant value for the reduction of the 4-NP over initial different concentration (c). ([4-NP] = 10–70 mg L^{-1}, [catalyst] = 0.5 g L^{-1}).

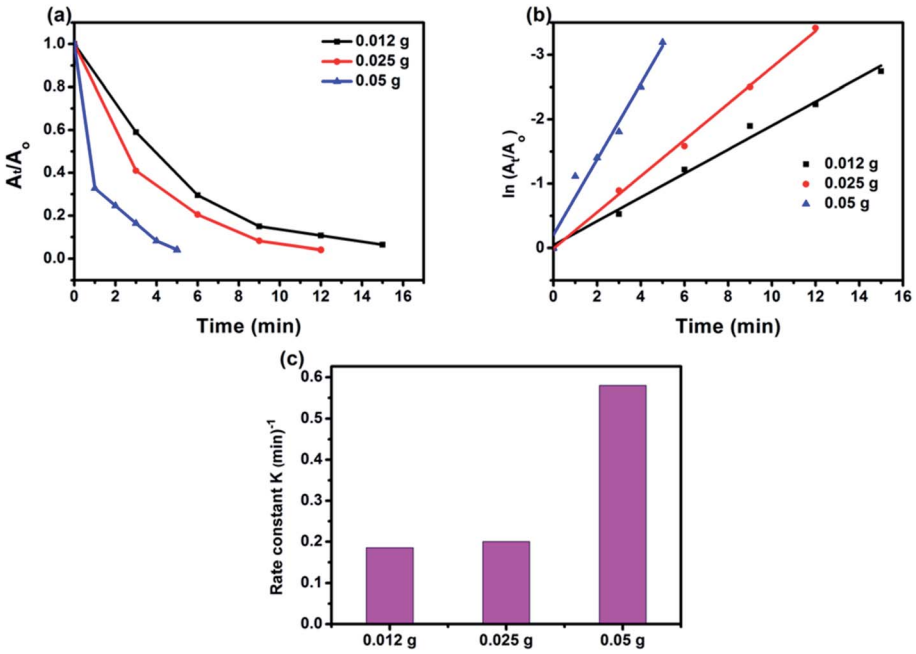

Fig. 9 Reduction rate of 4-NP over catalyst amount (a); corresponding linear transform $\ln(A_t/A_0) = f(t)$ of the 4-NP reduction kinetics curves (b); comparison of the rate constant value for the reduction of the 4-NP over catalyst amount (c). ([4-NP] = 70 mg L^{-1}, [catalyst] = 0.012–0.05 g in 50 mL [4-NP]).

increase to 0.05 g, the reduction efficiency value is 99% within 5 min for 4-NP reduction. The 50% $BiPO_4$/g-C_3N_4 composite (0.05 g) exhibited the highest rate constant of 0.58 min^{-1} compared with 0.025 g (0.26 min^{-1}), and 0.012 g (0.18 min^{-1}) catalyst dosage as shown in Fig. 9c. As above-discussed, the relationship between the active sites on the surface of the catalyst and 4-NP molecules is very significant in terms of reaction kinetics. The use of higher amount of catalyst is required to proceed a faster reduction reaction at high 4-NP concentration.

3.3 Feasible mechanism for 4-NP reduction

Overall, the obtained results showed that the bare g-C_3N_4 has very low catalytic efficiency towards the reduction of 4-NP from one side, and from another side, $BiPO_4$/g-C_3N_4 catalysts exhibited ultrafast catalytic reductive conversion of 4-NP, compared to bare $BiPO_4$. In addition, the higher amount $BiPO_4$ in the composite, the faster reduction kinetics. These results lead to deduce that $BiPO_4$ plays an important key especially when it is bonded to g-C_3N_4 nanosheets. The Langmuir–Hinshelwood (LH) model was proposed as mechanism for our

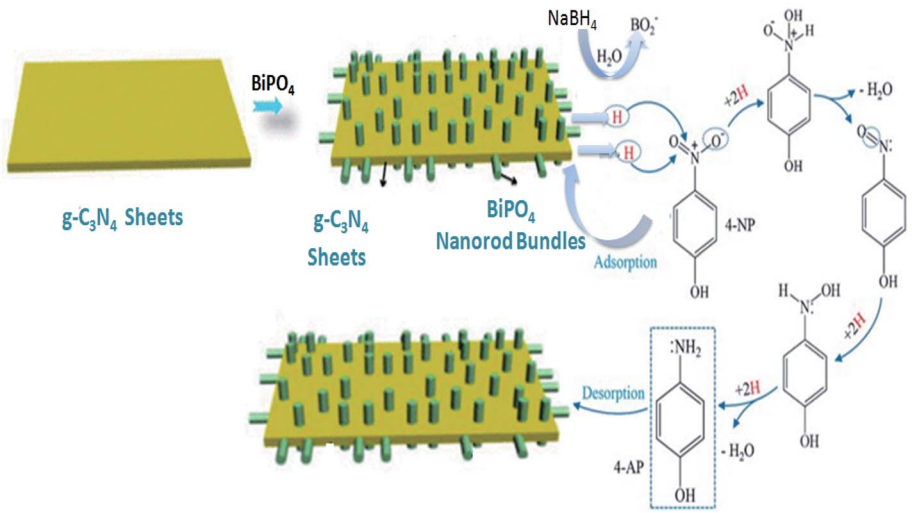

Scheme 2 The plausible mechanism for the catalytic reduction of 4-NP by $BiPO_4$/g-C_3N_4 composite using $NaBH_4$ as a reducing agent.

Table 3 The comparison of present work with the recent literature of catalytic reduction of 4-NP to 4-AP using various catalysts with its reaction conditions

Catalyst	Conc. of 4-NP (mol dm^{-3})	Conc. of $NaBH_4$ (mol dm^{-3})	Amount of catalyst (g L^{-1})	Time (min)	Rate constant (min^{-1})	Number of cycles	Ref.
g-C_3N_4/CuS	1.26×10^{-2}	0.5	3.3	50	0.0411	5	68
Au@g-C_3N_4	0.01	0.1	1	10	0.109	10	69
Au/CeO_2@g-C_3N_4	0.12×10^{-3}	0.04	0.5	0.6	6.36	5	27
g-C_3N_4/Bi_2S_3	0.03	0.2×10^{-3}	0.01	60	0.016	5	70
Cu@g-C_3N_4	0.13×10^{-3}	1.64×10^{-5}	5	25	1.11	4	71
N/graphene	0.1×10^{-3}	0.04×10^{-3}	1.5	18	0.029	3	72
Ag/g-C_3N_4/V_2O_5	0.01	0.5	5	60	0.373	3	73
50% $BiPO_4$/g-C_3N_4	7.18×10^{-5}	16×10^{-3}	0.5	1	2.914	5	This work

reaction. The plausible mechanism for the 4-NP in the presence of $NaBH_4$ and $BiPO_4$/g-C_3N_4 is shown in Scheme 2. $NaBH_4$ undergoes an ionization and produce BH_4^- species, which adsorb on the catalyst surface, followed by BO^{2-} species generation as a result of self-hydrolysis. Simultaneously, adsorbed BH_4^- species can induce the transfer of active hydrogen species to form hydride complex. Afterwards, such active hydrogen species react with nitro groups to reduce them into amino groups, as reported in previous studies.[66,67] The produced aminophenol is released from the surface of the catalyst to the medium. The catalytic reduction activity of $BiPO_4$/g-C_3N_4 composites were significantly enhanced compared with bare $BiPO_4$ and g-C_3N_4 due to addition of $BiPO_4$ nanorod bundles immobilized on the g-C_3N_4 nanosheets to form heterojunction system may form more active surface-hydrogen species, suggesting higher yield of 4-NP reduction. In addition, the conductive g-C_3N_4 can transfer electrons and $H^{\bullet}$ radicals from the adsorbed BH_4^- to 4-NP through the catalytic $BiPO_4$ nanorod bundles more readily, resulting in the production of 4-AP. Furthermore, the heterojunction of $BiPO_4$/g-C_3N_4 renders all active sites readily accessible that can significantly facilitate the rapid transport and diffusion of hydrogen radicals and electrons, resulting in the enhanced catalytic reduction on 4-NP. The efficiency of $BiPO_4$/g-C_3N_4 towards the reduction of 4-NP was comparatively listed in Table 3 with the recent previous reported catalysts for 4-NP reduction. The value of rate constant was calculated to be 2.914 min^{-1} for 50% $BiPO_4$/g-C_3N_4 nanocomposite that is much better than other nanocomposites, as shown in Table 3.

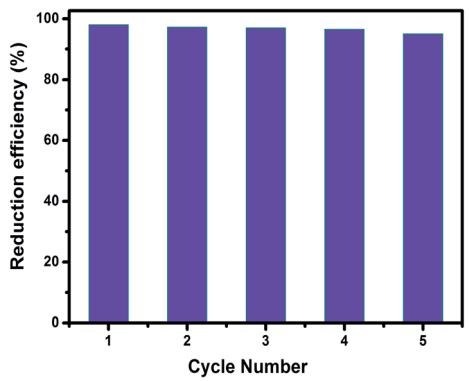

Fig. 10 Cyclic runs for the reduction of 4-NP on 50% $BiPO_4$/g-C_3N_4 heterojunction in the presence of $NaBH_4$. ([4-NP] = 50 mg L^{-1}, [catalyst] = 0.5 g L^{-1}).

3.4 Stability evaluation

Recycling of any heterogeneous catalyst has a significant role, especially for the economic and environmental points of view. The catalytic performance of $BiPO_4$/g-C_3N_4 catalyst was checked five times in a row towards the reduction of 4-NP under the same conditions (50 mg L^{-1}, and 25 mg 50% $BiPO_4$/g-C_3N_4). As shown in Fig. 10, the reduction rate was slightly decreased from 98% to 95%, after five times recycling. The results demonstrated that the as-prepared 50% $BiPO_4$/g-C_3N_4 heterojunction was comparably stable under the studied conditions, which is an advantage of using the catalysts for industrial applications.

4. Conclusions

Highly efficient and stable $BiPO_4$ nanorod bundles supported on g-C_3N_4 sheets composites with variable $BiPO_4$ loadings were developed using *ex situ* chemical deposition. The as synthesized composites showed superior catalytic activities towards reduction of 4-NP to 4-AP in wastewater, unlike bare g-C_3N_4 and $BiPO_4$. It was found that the increasing $BiPO_4$ loading enhanced catalytic reduction of 4-NP. The 50% $BiPO_4$/g-C_3N_4 sample performed the highest rate constant for 4-NP reduction which was 728.5 and 56 times superior than the values for g-C_3N_4 and $BiPO_4$, respectively. The mechanism for high-efficient catalytic activity have been discussed. In addition, the synthesized $BiPO_4$/g-C_3N_4 heterojunction does not show a significant reduce in its catalytic efficiency during the five times recycling tests. Therefore, the $BiPO_4$/g-C_3N_4 composite indicated the potential application for removing the hazardous wastes such as *p*-nitrophenol from the environment as a whole.

Conflicts of interest

There are no conflicts to declare.

Acknowledgements

We acknowledge the financial support from Helwan University and the Central Metallurgical Research and Development Institute (CMRDI).

References

1 T. Begildayeva, S. J. Lee, Y. Yu, J. Park, T. H. Kim, J. Theerthagiri, A. Ahn, H. J. Jung and M. Y. Choi, *J. Hazard. Mater.*, 2020, **409**, 124412.
2 Z. Zhu, L. Tao and F. Li, *J. Hazard. Mater.*, 2014, **279**, 436–443.
3 Z. Xiong, H. Zhang, W. Zhang, B. Lai and G. Yao, *Chem. Eng. J.*, 2019, **359**, 13–31.
4 Q. Chen, C. Ma, W. Duan, D. Lang and B. Pan, *J. Cleaner Prod.*, 2020, **271**, 122550.
5 M. I. Din, R. Khalid, Z. Hussain, T. Hussain, A. Mujahid, J. Najeeb and F. Izhar, *Crit. Rev. Anal. Chem.*, 2020, **50**, 322–338.
6 A. A. Pradhan and P. R. Gogate, *Chem. Eng. J.*, 2010, **156**, 77–82.
7 M. T. Qamar, M. Aslam, I. M. I. Ismail, N. Salah and A. Hameed, *ACS Appl. Mater. Interfaces*, 2015, **7**, 8757–8769.
8 S. R. Thawarkar, N. D. Khupse and A. Kumar, *ChemistrySelect*, 2017, **2**, 6833–6843.
9 A. Hernández-Gordillo, A. G. Romero, F. Tzompantzi and R. Gómez, *Appl. Catal., B*, 2014, **144**, 507–513.
10 M. A. Koklioti, T. Skaltsas, Y. Sato, K. Suenaga, A. Stergiou and N. Tagmatarchis, *Nanoscale*, 2017, **9**, 9685–9692.
11 M. Zhang, X. Su, L. Ma, A. Khan, L. Wang, J. Wang, A. S. Maloletnev and C. Yang, *J. Hazard. Mater.*, 2021, **403**, 123870.
12 P. Kar, K. Shukla, P. Jain, G. Sathiyan and R. K. Gupta, *Nano Mater. Sci.*, 2020, **3**, 25–46.
13 O. L. Stroyuk and S. Y. Kuchmy, *Theor. Exp. Chem.*, 2020, **56**, 143–173.
14 C. Liu, J. Li, Y. Li, W. Li, Y. Yang and Q. Chen, *RSC Adv.*, 2015, **5**, 71692–71698.
15 K. Hu, M. Yao, Z. Yang, G. Xiao, L. Zhu, H. Zhang, R. Liu, B. Zou and B. Liu, *Nanoscale*, 2020, **12**, 12300–12307.
16 C. Pan, J. Xu, Y. Wang, D. Li and Y. Zhu, *Adv. Funct. Mater.*, 2012, **22**, 1518–1524.
17 A. Mishra, A. Mehta, S. Basu, N. P. Shetti, K. R. Reddy and T. M. Aminabhavi, *Carbon*, 2019, **149**, 693–721.
18 C. Lu, P. Zhang, S. Jiang, X. Wu, S. Song, M. Zhu, Z. Lou, Z. Li, F. Liu, Y. Liu, Y. Wang and Z. Le, *Appl. Catal., B*, 2017, **200**, 378–385.
19 X. Chen, R. Shi, Q. Chen, Z. Zhang, W. Jiang, Y. Zhu and T. Zhang, *Nano Energy*, 2019, **59**, 644–650.
20 M. Wu, J.-M. Yan, X. Tang, M. Zhao and Q. Jiang, *ChemSusChem*, 2014, **7**, 2654–2658.
21 P. Su, J. Zhang, K. Xiao, S. Zhao, R. Djellabi, X. Li, B. Yang and X. Zhao, *Chin. J. Catal.*, 2020, **41**, 1894–1905.
22 D. Masih, Y. Ma and S. Rohani, *Appl. Catal., B*, 2017, **206**, 556–588.
23 X. Liu, R. Ma, L. Zhuang, B. Hu, J. Chen, X. Liu and X. Wang, *Crit. Rev. Environ. Sci. Technol.*, 2020, **51**, 751–790.
24 L. Zhou, H. Zhang, H. Sun, S. Liu, M. O. Tade, S. Wang and W. Jin, *Catal. Sci. Technol.*, 2016, **6**, 7002–7023.
25 K. Gu, X. Pan, W. Wang, J. Ma, Y. Sun, H. Yang, H. Shen, Z. Huang and H. Liu, *Small*, 2018, **14**, 1–8.
26 P. Fageria, S. Uppala, R. Nazir, S. Gangopadhyay, C. H. Chang, M. Basu and S. Pande, *Langmuir*, 2016, **32**, 10054–10064.
27 M. Kohantorabi and M. R. Gholami, *Appl. Phys. A: Mater. Sci. Process.*, 2018, **124**, 1–17.
28 Y. Y. Liu, Y. H. Zhao, Y. Zhou, X. L. Guo, Z. T. Chen, W. J. Zhang, Y. Zhang, J. Chen, Z. M. Wang, L. T. Sun and T. Zhang, *Nanotechnology*, 2018, **29**, 315702.
29 W. J. Ong, *Front. Mater.*, 2017, **4**, 1–10.
30 J. Wen, J. Xie, X. Chen and X. Li, *Appl. Surf. Sci.*, 2017, **391**, 72–123.
31 Y. Sang, X. Cao, G. Dai, L. Wang, Y. Peng and B. Geng, *J. Hazard. Mater.*, 2020, **381**, 120942.
32 Y. Li, H. Wang, L. Huang, C. Wang, Q. Wang, F. Zhang, X. Fan, M. Xie and H. Li, *J. Alloys Compd.*, 2020, **816**, 152665.
33 X. Ren, K. Wu, Z. Qin, X. Zhao and H. Yang, *J. Alloys Compd.*, 2019, **788**, 102–109.
34 S. Li, J. Chen, S. Hu, H. Wang, W. Jiang and X. Chen, *Chem. Eng. J.*, 2020, **402**, 126165.
35 R. A. Geioushy, S. M. El-Sheikh, A. B. Azzam, B. A. Salah and F. M. El-Dars, *J. Hazard. Mater.*, 2020, **381**, 120955.
36 L. Cheng, X. Hu and L. Hao, *Ultrason. Sonochem.*, 2018, **44**, 137–145.
37 C. Pan and Y. Zhu, *Catal. Sci. Technol.*, 2015, **5**, 3071–3083.
38 Y. Liu, W. Yao, D. Liu, R. Zong, M. Zhang, X. Ma and Y. Zhu, *Appl. Catal., B*, 2015, **163**, 547–553.
39 H. Lin, H. Ye, S. Chen and Y. Chen, *RSC Adv.*, 2014, **4**, 10968.
40 Y. Liu, P. Zhang, H. Lv, J. Guang, S. Li and J. Jiang, *RSC Adv.*, 2015, **5**, 83764–83772.
41 Y. Zhang, B. Shen, H. Huang, Y. He, B. Fei and F. Lv, *Appl. Surf. Sci.*, 2014, **319**, 272–277.
42 P. Hu, J. Niu, M. Yu and S. Y. Lin, *Chin. J. Anal. Chem.*, 2017, **45**, 357–362.
43 J. Li, H. Yuan and Z. Zhu, *Appl. Surf. Sci.*, 2016, **385**, 34–41.
44 Y. Lv, Y. Zhu and Y. Zhu, *J. Phys. Chem. C*, 2013, **117**, 18520–18528.
45 Y. Zhu, Q. Ling, Y. Liu, H. Wang and Y. Zhu, *Appl. Catal., B*, 2016, **187**, 204–211.
46 Y. Zhiu, Y. Liu, Y. Lv, Q. Ling, D. Liu and Y. Zhu, *J. Mater. Chem. A*, 2014, **2**, 13041–13048.
47 Y. Guo, P. Wang, J. Qian, J. Hou, Y. Ao and C. Wang, *Catal. Sci. Technol.*, 2018, **8**, 486–498.
48 Y. Wang, W. Luo, W. Jiang, Z. Wei and Y. Zhu, *Mater. Today Adv.*, 2019, **1**, 100006.
49 D. Long, Z. Chen, X. Rao and Y. Zhang, *ACS Appl. Energy Mater.*, 2020, **3**, 5024–5030.
50 X. Zou, C. Ran, Y. Dong, Z. Chen, D. Dong, D. Hu, X. Li and Y. Cui, *RSC Adv.*, 2016, **6**, 20664–20670.
51 A. B. Azzam, S. M. El-Sheikh, R. A. Geioushy, B. A. Salah, F. M. El-Dars and A. S. Helal, *RSC Adv.*, 2019, **9**, 17246–17253.
52 X. Zou, C. Ran, Y. Dong, Z. Chen, D. Dong, D. Hu, X. Li and Y. Cui, *RSC Adv.*, 2016, **6**, 20664–20670.

53 Z. Li, S. Yang, J. Zhou, D. Li, X. Zhou, C. Ge and Y. Fang, *Chem. Eng. J.*, 2014, **241**, 344–351.
54 M. H. Fulekar, A. Singh, D. P. Dutta, M. Roy, A. Ballal and A. K. Tyagi, *RSC Adv.*, 2014, **4**, 10097–10107.
55 S. M. El-Sheikh, A. B. Azzam, R. A. Geioushy, F. M. El Dars and B. A. Salah, *J. Alloys Compd.*, 2021, **857**, 157513.
56 L. She, G. Tan, H. Ren, J. Huang, C. Xu and A. Xia, *RSC Adv.*, 2015, **5**, 36642.
57 J. Zhao, Q. Han, J. Zhu, X. Wu and X. Wang, *Nanoscale*, 2014, **6**, 10062–10070.
58 R. Djellabi, B. Yang, K. Xiao, Y. Gong, D. Cao, H. M. A. Sharif, X. Zhao, C. Zhu and J. Zhang, *J. Colloid Interface Sci.*, 2019, **553**, 409–417.
59 J. Xia, J. Zhao, J. Chen, J. Di, M. Ji, L. Xu, Z. Chen and H. Li, *J. Photochem. Photobiol., A*, 2017, **339**, 59–66.
60 Q. Liang, J. Jin, C. Liu, S. Xu, C. Yao and Z. Li, *J. Mater. Sci.: Mater. Electron.*, 2018, **29**, 2509–2516.
61 H. Sun, G. Zhou, Y. Wang, A. Suvorova and S. Wang, *ACS Appl. Mater. Interfaces*, 2014, **6**, 16745–16754.
62 J. Gao, J. Wang, X. Qian, Y. Dong, H. Xu, R. Song, C. Yan, H. Zhu, Q. Zhong, G. Qian and J. Yao, *J. Solid State Chem.*, 2015, **228**, 60–64.
63 M. T. Shah, A. B. Sirajuddin, A. Ahmed, P. Abdullah, A. Muhammad, M. Saman, R. Khattak and A. Ali, *Microsyst. Technol.*, 2017, **23**, 5745–5758.
64 S. R. Thawarkar, B. Thombare, B. S. Munde and N. D. Khupse, *RSC Adv.*, 2018, **8**, 38384–38390.
65 G. Wu, X. Liang, L. Zhang, Z. Tang, M. Al-Mamun, H. Zhao and X. Su, *ACS Appl. Mater. Interfaces*, 2017, **9**, 18207–18214.
66 Y. Fu, P. Xu, D. Huang, G. Zeng, C. Lai, L. Qin, B. Li, J. He, H. Yi, M. Cheng and C. Zhang, *Appl. Surf. Sci.*, 2019, **473**, 578–588.
67 D. Ayodhya and G. Veerabhadram, *J. Mol. Struct.*, 2019, **1186**, 423–433.
68 D. Ayodhya and G. Veerabhadram, *FlatChem*, 2019, **14**, 100088.
69 T. B. Nguyen, C. P. Huang and R. an Doong, *Appl. Catal., B*, 2019, **240**, 337–347.
70 D. Ayodhya and G. Veerabhadram, *Environ. Technol.*, 2019, **42**, 826–841.
71 S. Huang, Y. Zhao and R. Tang, *RSC Adv.*, 2016, **6**, 90887–90896.
72 P. V. R. K. Ramacharyulu, S. J. Abbas, S. R. Sahoo and S. C. Ke, *Catal. Sci. Technol.*, 2018, **8**, 2825–2834.
73 H. S. EL-Sheshtawy, H. M. El-Hosainy, K. R. Shoueir, I. M. El-Mehasseb and M. El-Kemary, *Appl. Surf. Sci.*, 2019, **467–468**, 268–276.